2021 American Control Conference (ACC)
New Orleans, USA, May 25-28, 2021

A Laplacian Regularized Least Square Algorithm for Motion Tomography

Meriam Ouerghi and Fumin Zhang

Abstract— **The motion of an Autonomous Underwater Vehicle (AUV) is often affected by unknown disturbances arising from underwater flow fields. These disturbances may result in large prediction errors when comparing the AUV's expected surfacing location (for example from dead reckoning) and the AUV's measured surfacing location. This error, referred to as the Motion Integration Error, has been used by Motion Tomography algorithm (MT) to reconstruct an estimate of the underwater flow field. In this paper, we extend the MT algorithm to solve the MT problem by introducing Laplacian regularization that penalizes the non-smoothness of the predicted flow field. We propose an iterative algorithm to solve the Regularized MT (RMT) problem. The convergence of the RMT algorithm in the single vehicle case is theoretically justified. The effectiveness of the algorithm for multiple vehicle applications is validated through simulations with cyclonic flow field models. We show that the RMT algorithm outperforms the parametric MT in terms of estimation accuracy and convergence rate.**

I. Introduction

Due to the lack of accurate position measurements (for example from a global positioning service), Autonomous Underwater Vehicle (AUV) navigation depends on an accurate estimate of the spatially-distributed underwater disturbances, also known as a flow field. Several algorithms have been proposed in the literature that embed flow measurements and ocean flow field predictions in order to enable AUV path planning [1]. However, existing ocean flow models suffer from coarse resolution, making their applicability in AUV deployment minimal [2]. More recent work leverages the AUV motion response to estimate the flow field, supported by sensors onboard the vehicles [3], [4]. A specialized Gaussian process regression scheme that exploits the incompressibility of ocean currents was proposed in [5] and a nonlinear observer was designed to identify an unknown vector field parameterized by basis functions in [6]. However, these methods require a prior model of the flow field or in-situ flow velocity observations to counteract the underdetermined nature of the problem.

In our previous work, we used the motion integration error to create a high resolution flow field model [7], [8]. Our approach is inspired by inverse problems in tomography theory in which the error is described by the difference in a GPS measured surfacing position and a predicted surfacing position. The approach leverages the motion integration error to infer the underlying flow field.

In general nonlinear tomography, inverse problems, such as in seismic tomography, are usually ill-posed making it difficult to find accurate solutions [9], [10]. In order to overcome this issue, different regularization strategies have been proposed in [11]. In addition, Gaussian radial basis functions have also been used in [7] for a parametric flow estimation. However, such implicit regularization tends to under fit the data and favors an uniform flow field. Therefore, the Gaussian radial basis function parametric MT predicts less accurate results in comparison with the non parametric MT when the flow is highly varying over the spatial domain. A better solution is piecewise discretization, which can approximate a large class of functions and do not embed a prior model in the prediction. Therefore, it can capture the flow dynamics better than the parametric MT.

While gradient-based methods have been applied to solve nonlinear inverse problems [12] [10], the motion tomography problem is non-differentiable due to the piecewise discretization, which renders gradient-based approaches inapplicable in our problem. Therefore, we proposed an iterative solution that combines trajectory tracing and flow field estimation to solve the MT problem. Starting from an initial guess of the flow field, the AUV trajectory and the travel time weight matrix are computed to update the flow estimate [7]. We also derived in our previous work an analytical expression for trajectory tracing that we used to prove the convergence of the MT algorithm for a single AUV trajectory [13].

In this paper, we aim to alleviate the ill-posedness of the inverse problem in piecewise discrete nonlinear tomography by adding the Laplacian regularization in the MT objective function. In the MT problem, the number of AUVs is limited and the MT algorithm might generate a highly varying flow field. To address this problem, we use the Laplacian regularized least square (LapRLS) and we call the proposed algorithm Regularized Motion Tomography. LapRLS is a special case of the manifold regularization, which enforces smoothness of solutions relative to the underlying manifold by preserving the local geometrical structure of the data space [14], [15]. Replacing the unknown manifold Laplacian with the graph Laplacian results in the Laplacian regularized least squares, which is an effective semi-supervised learning algorithm that can measure the variability of the predictor with respect to the empirical distribution. Therefore, it is reasonable to apply the Laplacian regularization which favors a relatively smooth solution and reflects the spatial variation of the flow better than the parametric MT.

The research work is supported by ONR grants N00014-19-1-2556 and N00014-19-1-2266; NSF grants OCE-1559475, CNS-1828678, and SAS-1849228; NRL grants N00173-17-1-G001 and N00173-19-P-1412; and NOAA grant NA16NOS0120028.

Meriam Ouerghi and Fumin Zhang are with the School of Electrical and Computer Engineering, Georgia Institute of Technology, Atlanta, Georgia 30332, USA {mouerghi3,fumin}@gatech.edu

978-1-6654-4197-1/$31.00 ©2021 AACC

Further, we study the flow field dynamics as the RMT algorithm proceeds. This allows us to derive the RMT error dynamics, taking into account the regularization term. We analyze the RMT properties and prove the convergence of the RMT algorithm in the single vehicle case. Finally, we validate our approach for multiple vehicles via simulations using cyclonic flow field models. The simulations show that the RMT algorithm can reconstruct the flow field without any prior information and outperforms both the non-parametric and Gaussian Radial basis function parametric MT algorithm. Our proposed method can also be extended to solve general nonlinear inverse problems where the Jacobian is not defined, which impedes the application of gradient-based methods.

The rest of the paper is organized as follows. In Section II, we introduce the Motion Tomography problem and we formulate the RMT solution in III. In Section IV, we derive the flow estimation dynamics and prove the RMT algorithm's convergence. Simulation results comparing the proposed algorithm with previous work are provided in Section V. Finally, a summary of the paper and future work is given in SectionVI.

II. PROBLEM SETUP AND MOTION TOMOGRAPHY

In this section we model the influence of the flow on the vehicle trajectory and explain the MT problem. We consider the AUV horizontal position $\tilde{r}(t) \in \mathbb{R}^2$ in the presence of the ambient flow $\tilde{F}(\tilde{r}(t)) = [\tilde{F}_x(\tilde{r}(t)), \tilde{F}_y(\tilde{r}(t))] \in \mathbb{R}^2$ and we model the AUV motion using a first order particle model with constant control velocity $S \in \mathbb{R}^2$. The net velocity $\tilde{V}(t)$ is the sum of the control velocity and the flow velocity: $\tilde{V}(t) = S + \tilde{F}(\tilde{r}(t))$. Let $r(0) \in \mathbb{R}^2$ be the initial position and t^{tot} be the total travel time, then the AUV final position $\tilde{r}(t^{\text{tot}}) \in \mathbb{R}^2$ satisfies:

$$\tilde{r}(t^{\text{tot}}) = \tilde{r}(0) + \int_0^{t^{tot}} \Big(S + \tilde{F}(\tilde{r}(t))\Big)\,\mathrm{dt} \tag{1}$$

We simplify the problem formulation by making the following assumption.

Assumption 1: The control velocity S is known and the flow field is time-invariant during $t = [0, t^{tot}]$.

Remark 1: As the travel time interval t^{tot} is typically several hours, the difference between the true and the assigned control velocity is usually negligible. Further, we can reduce t^{tot} such that the error caused by a time-varying flow field is minimal. Thus the assumption usually holds for realistic AUV applications, see [7].

Suppose $F(r)$ is an initial estimate of the true flow field $\tilde{F}(\tilde{r})$, then the predicted final position $r(t^{\text{tot}})$ follows:

$$r(t^{\text{tot}}) = \tilde{r}(0) + \int_0^{t^{tot}} (S + F(r(t)))\,\mathrm{dt} \tag{2}$$

While the AUV position can be measured at times t^0 and t^{tot}, the true flow $\tilde{F}(r)$ is unknown. Hence, an offset between the estimated final position $r(t^{\text{tot}})$ and the measured final position $\tilde{r}(t^{\text{tot}})$ is observed. We refer to this offset as the motion integration error, defined using equations (1) and (2) as follows:

$$d = \tilde{r}(t^{\text{tot}}) - r(t^{\text{tot}}) = \int_0^{t^{tot}} \Big(\tilde{F}(\tilde{r}(t)) - F(r(t))\Big)\,\mathrm{dt}.$$

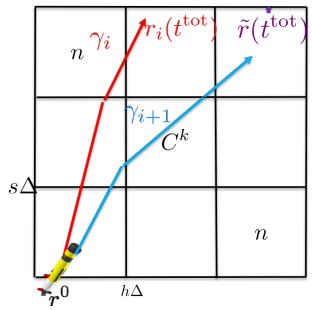

Fig. 1: Illustration of MT mapping formulation. The predicted trajectories γ_i and γ_{i+1} are displayed in a discretized domain.

A. The MT Problem

The MT method computes a map of the flow field F such that $d = 0$. Let us discretize a domain $\mathcal{D}$ into $P = n \times n$ grid cells with C^k referring to the $k^{th} = h + s * n$ cell that exists in the h^{th} column and the s^{th} row , $1 \le k \le P$, as illustrated in Fig.1. We assume the flow field within C^k is constant and we denote the estimated flow by $F^k = [F_x^k, F_y^k]$.

Let N be the number of AUVs and r^j, $j = \{1, \cdots, N\}$ their positions in domain $\mathcal{D}$. We denote with $t^{j,k}$ the travel time that AUV j spent in cell C^k. Hence, $r^j(t^{\text{tot}})$ follows:

$$r^j(t^{\text{tot}}) = \tilde{r}^j(0) + \sum_{k=1}^{P} t^{j,k}\left(S^j + F^k\right). \tag{3}$$

Let $\mathbf{F}_x = [F_x^1, \cdots, F_x^P]^\top$,$\mathbf{F}_y = [F_y^1, \cdots, F_y^P]^\top$ and $\mathbf{F} = [\mathbf{F}_x, \mathbf{F}_y]$ be the flow field estimate. Further, we denote with $T^j = [t^{j,1}, \cdots, t^{j,P}]^\top$ the travel time vector where $t^{j,1}$ is the travel time that the AUV j spends in cell C^1. Given $\mathbf{F}$, we can compute T^j using trajectory tracing mechanism introduced in [7]. We rewrite (3) as follows:

$$r^j(t^{\text{tot}}) = \tilde{r}^j(0) + t^{\text{tot}} S^j + {T^j}^\top \mathbf{F} \tag{4}$$

Let $\tilde{\mathbf{F}}$ be the true flow field and $\tilde{T}^j$ the true travel time, then $\tilde{r}^j(t^{\text{tot}})$ follows:

$$\tilde{r}^j(t^{\text{tot}}) = \tilde{r}^j(0) + t^{\text{tot}} S^j + {\tilde{T}^j}^\top \tilde{\mathbf{F}} \tag{5}$$

Combining (4) and (5) leads to MT error d^j for AUV j:

$$d^j = {\tilde{T}^j}^\top \tilde{\mathbf{F}} - {T^j}^\top \mathbf{F} \tag{6}$$

Let $\mathbf{T} \in \mathbb{R}^{N \times P}$ be the travel time matrix and $\mathbf{d} \in \mathbb{R}^{N \times 2}$ the MT error for all AUVs, we construct $\mathbf{T} = [T^1, \cdots, T^N]$, $\tilde{\mathbf{T}} = [\tilde{T}^1, \cdots, \tilde{T}^N]$, $\mathbf{d}_x = [d_x^1, \cdots, d_x^N]^\top$ and $\mathbf{d}_y = [d_y^1, \cdots, d_y^N]^\top$, $\mathbf{d} = [\mathbf{d}_x, \mathbf{d}_y] = \tilde{\mathbf{T}}^\top \tilde{\mathbf{F}} - \mathbf{T}^\top \mathbf{F}$, $\tilde{\mathbf{F}}$ and $\mathbf{F}$ are the true and predicted flow. The MT problem is to compute $\mathbf{F}$ that minimizes the MT error norm:

$$\mathbf{F}_x^* = \underset{\mathbf{F}_x}{\operatorname{argmin}} \frac{1}{2}\|\mathbf{d}_x\|^2, \quad \mathbf{F}_y^* = \underset{\mathbf{F}_y}{\operatorname{argmin}} \frac{1}{2}\|\mathbf{d}_y\|^2 \tag{7}$$

B. The MT Solution

As the flow field is spatially variant, the travel time matrix $\mathbf{T}(\mathbf{F})$ is a nonlinear function with respect to the flow $\mathbf{F}$ and accordingly the optimization problem (7) is nonlinear. Recall that $\mathbf{F}$ is piecewise-constant, then Eq. (7) is not differentiable. Thus, gradient based methods can not be applied to solve (7). To deal with the nonlinearity in (7), we proposed an iterative solution, [13] to correct the flow estimate using all AUV trajectories simultaneously. Given an estimate of the flow $\mathbf{F}_i$ at iteration i, the travel time matrix $\mathbf{T}$ is computed using $\mathbf{F}_i$ to linearize Eq.(7). Hence, $\mathbf{F}_{i+1}$ is estimated

$$\mathbf{F}_{i+1} = \mathbf{F}_i + \omega \frac{\mathbf{T}(\mathbf{F}_i)\mathbf{d}_i}{\|\mathbf{T}(\mathbf{F}_i)\|^2} \tag{8}$$

where $0 < \omega < 1$ is a designed step-size parameter and $\|\mathbf{T}(\mathbf{F}_i)\| = \sigma(\mathbf{T}(\mathbf{F}_i)^\top \mathbf{T}(\mathbf{F}_i))^{\frac{1}{2}}$ is the spectral norm. The flow update (8) requires the MT error $\mathbf{d}_i$ and the travel time $\mathbf{T}(\mathbf{F}_i)$. Hence, we need to compute the AUV trajectories γ_i^j using the last estimate $\mathbf{F}_i$ to update $\mathbf{d}_i$ and $\mathbf{T}(\mathbf{F}_i)$.

Consider the travel time matrix $\mathbf{T}$, the (k, j)th entry indicates the contribution of flow k.th to the j.th projection measurement d^j. As the number of trajectories N is significantly less than the number of cells P, $\mathbf{T}$ is a sparse rank deficient matrix. Therefore, the MT inverse problem is a discrete ill-posed problem. To address this difficulty, we propose the Regularized Motion Tomography (RMT).

III. Regularized Motion Tomography

Given that the flow is a piecewise constant function, the MT algorithm exhibits flow differences between cells that are crossed by different AUV trajectories. While the total variation regularization generates piecewise constant structures, the Laplacian regularizer favors smooth solutions. Therefore, we apply the Laplacian regularizer to improve the smoothness of the estimated field.

We denote with $\mathbf{R} \in \mathbb{R}^{P \times P}$ the discrete Laplace operator. Thus $\mathbf{R}$ is positive semi-definite and its null space is 1-dimensional and spanned by the vector $\mathbf{1}$ [16].

Remark 2: For clarity, let $\mathbf{T}_i = \mathbf{T}(\mathbf{F}_i)$ and notice that ${\mathbf{T}_i}^\top \mathbf{T}_i$ and $\lambda \mathbf{R}^\top \mathbf{R}$ are positive semi-definite, therefore, so is the quantity $({\mathbf{T}_i}^\top \mathbf{T}_i + \lambda \mathbf{R}^\top \mathbf{R})$. Since ${\mathbf{T}_i}^\top \mathbf{1} = t^{\text{tot}} \neq 0$, and the null space of $\mathbf{R}$ is $\mathbf{1}$, then the eigenvalues of $({\mathbf{T}_i}^\top \mathbf{T}_i + \lambda \mathbf{R}^\top \mathbf{R})$ are positive and $({\mathbf{T}_i}^\top \mathbf{T}_i + \lambda \mathbf{R}^\top \mathbf{R})$ is invertible.

LapRLS is a special case of the manifold regularization framework, which preserves the local geometry of the data space [14]. As we can measure the AUV position only at t^{tot}, the number of trajectories is insufficient for an accurate estimation. To address this problem, we use the Laplacian graph penalty term that measures the spatial variation of the flow. Hence, adding this regularization cost improves the prediction and smoothes the flow estimate.

We modify the MT cost function with the Laplacian regularizer term as follows:

$$\mathbf{F}_{x,i+1} = \underset{\mathbf{F}_x}{\operatorname{argmin}} \frac{1}{2}\|\tilde{\mathbf{T}}^\top \tilde{\mathbf{F}}_x - \mathbf{T}^\top \mathbf{F}_x\|^2 + \frac{\lambda}{2}\|\mathbf{R}\mathbf{F}_x\|^2$$

$$\mathbf{F}_{y,i+1} = \underset{\mathbf{F}_y}{\operatorname{argmin}} \frac{1}{2}\|\tilde{\mathbf{T}}^\top \tilde{\mathbf{F}}_y - \mathbf{T}^\top \mathbf{F}_y\|^2 + \frac{\lambda}{2}\|\mathbf{R}\mathbf{F}_y\|^2 \tag{9}$$

where λ is a positive regularization parameter which controls the trade-off between a good fit to the measured data and the regularized solution. Contrary to the LapRLS proposed in [14], the cost function in Eq.(9) is nonlinear because the travel time matrix $\mathbf{T}$ depends on $\mathbf{F}$. Therefore we use an iterative algorithm to solve Eq.(9). Inserting $\mathbf{d}_i = \tilde{\mathbf{T}}^\top \tilde{\mathbf{F}} - \mathbf{T}_i^\top \mathbf{F}$ and $\mathbf{F} = \mathbf{F}_i + \Delta\mathbf{F}$ in (9) leads to:

$$\Delta\mathbf{F}_{x,i} = \underset{\Delta\mathbf{F}_{x,i}}{\operatorname{argmin}} \frac{1}{2}\|\mathbf{d}_{x,i} - \mathbf{T}_i^\top \Delta\mathbf{F}_x\|^2 + \frac{\lambda}{2}\|\mathbf{R}(\mathbf{F}_{x,i} + \Delta\mathbf{F}_x)\|^2$$

$$\Delta\mathbf{F}_{y,i} = \underset{\Delta\mathbf{F}_{y,i}}{\operatorname{argmin}} \frac{1}{2}\|\mathbf{d}_{y,i} - \mathbf{T}_i^\top \Delta\mathbf{F}_y\|^2 + \frac{\lambda}{2}\|\mathbf{R}(\mathbf{F}_{y,i} + \Delta\mathbf{F}_y)\|^2 \tag{10}$$

Setting the gradient of (10) to zero and given $({\mathbf{T}_i}^\top \mathbf{T}_i + \lambda \mathbf{R}^\top \mathbf{R})$ is invertible, then the optimal solution for (10) is:

$$\Delta\mathbf{F}_i = ({\mathbf{T}_i}^\top \mathbf{T}_i + \lambda \mathbf{R}^\top \mathbf{R})^{-1}(\mathbf{T}_i \mathbf{d}_i - \lambda \mathbf{R}^\top \mathbf{R}\mathbf{F}_i)$$

Since the original problem is nonlinear, we update $\mathbf{F}_{i+1}$

$$\mathbf{F}_{i+1} = \mathbf{F}_i + \omega \Delta\mathbf{F}_i \tag{11}$$

where $0 < \omega < 1$ is an appropriate step-length. The regularized MT algorithm follows:

Algorithm 1: RMT flow field estimation

Data: Measured final position $\tilde{r}^j(t^{\text{tot}}), j \in [1, \cdots N]$

Set $i = 0$. Make an initial guess of the solutions $\mathbf{F}_0$;

repeat

  Trajectory tracing (2) to get $\mathbf{T}_i$ and $\mathbf{d}_i$

  Update the flow in all cells k

$$\Delta\mathbf{F}_i = (\mathbf{T}_i {\mathbf{T}_i}^\top + \lambda \mathbf{R}^\top \mathbf{R})^{-1}(\mathbf{T}_i \mathbf{d}_i - \lambda \mathbf{R}^\top \mathbf{R}\mathbf{F}_i)$$

$$\mathbf{F}_{i+1} = \mathbf{F}_i + \omega \Delta\mathbf{F}_i \tag{12}$$

until $\|\Delta \boldsymbol{F}_i\| \leq \epsilon$

IV. Convergence Analysis of RMT

For theoretical analysis, we will focus on the single vehicle case. The nonlinear relationship between the AUV trajectories leads to some difficulties in the multi-vehicle analysis. Therefore, we will prove convergence of the algorithm for the multi-vehicle case in future work.

A. RMT Error Dynamics

In order to study the dynamics of $\mathbf{F}_i$ as the algorithm proceeds, we denote with $\hat{r} = [\hat{r}_x, \hat{r}_y] = \tilde{\mathbf{T}}^\top \tilde{\mathbf{F}}$. Further, let $\mathbf{I} \in \mathbb{R}^P$ such that $\mathbf{I} = [1, \cdots, 1]^\top$, $\mathbf{Y}_x = \frac{\hat{r}_x}{t^{\text{tot}}}\mathbf{I}$, $\mathbf{Y}_y = \frac{\hat{r}_y}{t^{\text{tot}}}\mathbf{I}$ and $\mathbf{Y} = [\mathbf{Y}_x, \mathbf{Y}_y]$. We compute in the following lemma an analytical expression of $\mathbf{F}_i$ as a function of $\mathbf{F}_0$.

Lemma 1: Let the flow be updated according to (12), then:

$$\mathbf{F}_{i+1} = (1-\omega)^{i+1}\mathbf{F}_0 + (1 - (1-\omega)^{i+1})\mathbf{Y} \tag{13}$$

Proof: Apply $\mathbf{d}_i = \tilde{\mathbf{T}}^\top \tilde{\mathbf{F}} - \mathbf{T}_i^\top \mathbf{F}_i$ in the flow update (12):

$$\begin{aligned}\Delta\mathbf{F}_i &= (\mathbf{T}_i\mathbf{T}_i{}^\top + \lambda\mathbf{R}^\top\mathbf{R})^{-1}(\mathbf{T}_i\mathbf{d}_i - \lambda\mathbf{R}^\top\mathbf{R}\mathbf{F}_i)\\ &= (\mathbf{T}_i\mathbf{T}_i{}^\top + \lambda\mathbf{R}^\top\mathbf{R})^{-1}(\mathbf{T}_i\tilde{\mathbf{T}}^\top\tilde{\mathbf{F}} - (\mathbf{T}_i\mathbf{T}_i^\top + \lambda\mathbf{R}^\top\mathbf{R})\mathbf{F}_i)\\ &= -\mathbf{F}_i + (\mathbf{T}_i\mathbf{T}_i{}^\top + \lambda\mathbf{R}^\top\mathbf{R})^{-1}\mathbf{T}_i\tilde{\mathbf{T}}^\top\tilde{\mathbf{F}} \qquad (14)\end{aligned}$$

Insert $\mathbf{M}_i = (\mathbf{T}_i\mathbf{T}_i{}^\top + \lambda\mathbf{R}^\top\mathbf{R})^{-1}$ in (14), then $\mathbf{F}_{i+1}$ follows:

$$\mathbf{F}_{i+1} = \mathbf{F}_i + \omega\Delta\mathbf{F}_i = (1-\omega)\mathbf{F}_i + \omega\mathbf{M}_i\mathbf{T}_i\tilde{\mathbf{T}}^\top\tilde{\mathbf{F}} \qquad (15)$$

Recall that $\mathbf{R}^\top\mathbf{R}\mathbf{I} = \mathbf{0}$ and $\mathbf{Y} = [\mathbf{Y}_x, \mathbf{Y}_y]$ where $\mathbf{Y}_x = \frac{\hat{r}_x}{t^{\text{tot}}}\mathbf{I}$ and $\mathbf{Y}_y = \frac{\hat{r}_y}{t^{\text{tot}}}\mathbf{I}$, then $\mathbf{R}^\top\mathbf{R}\mathbf{Y} = \mathbf{0}$ and $\mathbf{M}_i^{-1}\mathbf{Y}_x$ follows:

$$\begin{aligned}\mathbf{M}_i^{-1}\mathbf{Y}_x &= (\mathbf{T}_i\mathbf{T}_i{}^\top + \lambda\mathbf{R}^\top\mathbf{R})\mathbf{Y}_x\\ &= \mathbf{T}_i\mathbf{T}_i{}^\top\mathbf{Y}_x = \frac{\hat{r}_x}{t^{\text{tot}}}\mathbf{T}_i\mathbf{T}_i{}^\top\mathbf{I} \qquad (16)\end{aligned}$$

Insert $\hat{r}_x = \tilde{\mathbf{T}}^\top\tilde{\mathbf{F}}_x$ in Eq.(16), results in the following:

$$\mathbf{M}_i^{-1}\mathbf{Y}_x = \frac{1}{t^{\text{tot}}}\mathbf{T}_i\tilde{\mathbf{T}}^\top\tilde{\mathbf{F}}_x\mathbf{T}_i^\top\mathbf{I} \qquad (17)$$

Insert $\mathbf{T}_i^\top\mathbf{I} = t^{\text{tot}}$ and multiply both sides with $\mathbf{M}_i$:

$$\mathbf{M}_i\mathbf{T}_i\tilde{\mathbf{T}}^\top\tilde{\mathbf{F}}_x = \mathbf{Y}_x \qquad (18)$$

The same steps for $\mathbf{Y}_y$ leads to $\mathbf{M}_i\mathbf{T}_i\tilde{\mathbf{T}}^\top\tilde{\mathbf{F}}_y = \mathbf{Y}_y$. Hence $\mathbf{M}_i\mathbf{T}_i\tilde{\mathbf{T}}^\top\tilde{\mathbf{F}} = \mathbf{Y}$ As $\mathbf{Y} = [\frac{\hat{r}_x}{t^{\text{tot}}}, \frac{\hat{r}_y}{t^{\text{tot}}}]\mathbf{I}$, then $\mathbf{Y}$ is a constant vector that represents the average flow field along the AUV trajectory. Now we can rewrite (15) as follows:

$$\mathbf{F}_{i+1} = (1-\omega)^{i+1}\mathbf{F}_0 + \omega\sum_{j=0}^{i}(1-\omega)^j\mathbf{Y}$$

Apply the geometric sum, then $\omega\sum_{j=0}^{i}(1-\omega)^j = (1-(1-\omega)^{i+1})$ and $\mathbf{F}_{i+1}$ follows:

$$\mathbf{F}_{i+1} = (1-\omega)^{i+1}\mathbf{F}_0 + (1-(1-\omega)^{i+1})\mathbf{Y}$$

■

Since the regularization term penalizes the flow difference between cells, we define $\mathbf{Z}_i = \sqrt{\lambda}\mathbf{R}\mathbf{F}_i$ as the estimate of the flow variation and we expand the RMT state vector as $\mathbf{X}_i = [\mathbf{d}_i, \mathbf{Z}_i]^\top$. Now we derive the dynamics of the $\mathbf{X}_i$.

Lemma 2: Let the flow be updated according to (12), then $\mathbf{X}_i$ evolves according to the following dynamics:

$$\mathbf{X}_{i+1} = \mathbf{A}_i\mathbf{X}_i + \mathbf{B}_i \qquad (19)$$

where

$$\mathbf{A}_i = \begin{bmatrix} I - \omega\mathbf{T}_i^\top\mathbf{M}_i\mathbf{T}_i & \omega\sqrt{\lambda}\mathbf{T}_i^\top\mathbf{M}_i\mathbf{R}^\top \\ \omega\sqrt{\lambda}\mathbf{R}\mathbf{M}_i\mathbf{T}_i & I - \omega\lambda\mathbf{R}\mathbf{M}_i\mathbf{R}^\top \end{bmatrix}. \qquad (20)$$

$\mathbf{M}_i = (\mathbf{T}_i\mathbf{T}_i{}^\top + \lambda\mathbf{R}^\top\mathbf{R})^{-1}$, $\mathbf{B}_i = [\mathbf{C}_{i+1}, \mathbf{0}]^\top$ and $\mathbf{C}_{i+1} = (\mathbf{T}_i - \mathbf{T}_{i+1})^\top\mathbf{F}_{i+1}$.

Proof: Consider the flow update and insert $\mathbf{Z}_i = \sqrt{\lambda}\mathbf{R}\mathbf{F}_i$ in Eq. (12) :

$$\mathbf{F}_{i+1} = \mathbf{F}_i + \omega\mathbf{M}_i(\mathbf{T}_i\mathbf{d}_i - \sqrt{\lambda}\mathbf{R}^\top\mathbf{Z}_i) \qquad (21)$$

Apply $\sqrt{\lambda}\mathbf{R}$ on both sides of Eq. (21) leads to $\mathbf{Z}_{i+1}$:

$$\mathbf{Z}_{i+1} = \mathbf{Z}_i + \omega\sqrt{\lambda}\mathbf{R}\mathbf{M}_i(\mathbf{T}_i\mathbf{d}_i - \sqrt{\lambda}\mathbf{R}^\top\mathbf{Z}_i) \qquad (22)$$

Consider the MT error $\mathbf{d}_{i+1}$ as follows:

$$\mathbf{d}_{i+1} = \tilde{\mathbf{T}}^\top\tilde{\mathbf{F}} - \mathbf{T}_i^\top\mathbf{F}_{i+1} - (\mathbf{T}_{i+1} - \mathbf{T}_i)^\top\mathbf{F}_{i+1} \qquad (23)$$

Inserting (21) in the first part of Eq.(23) leads to:

$$\begin{aligned}\mathbf{d}_{i+1} &= \tilde{\mathbf{T}}^\top\tilde{\mathbf{F}} - \mathbf{T}_i^\top(\mathbf{F}_i + \omega\mathbf{M}_i(\mathbf{T}_i\mathbf{d}_i - \sqrt{\lambda}\mathbf{R}^\top\mathbf{Z}_i)) + \mathbf{C}_{i+1}\\ &= \mathbf{d}_i - \omega\mathbf{T}_i^\top\mathbf{M}_i(\mathbf{T}_i\mathbf{d}_i - \sqrt{\lambda}\mathbf{R}^\top\mathbf{Z}_i) + \mathbf{C}_{i+1} \qquad (24)\end{aligned}$$

Combining Eq. (23) and (24) results in Eq. (19) and (20). ■

In order to show the convergence of the RMT algorithm, we derive in the following Lemma an upper bound on the norm of the transition matrix $\mathbf{A}_i$ when $\Delta\mathbf{F}_i \neq \mathbf{0}$. We will address the case $\Delta\mathbf{F}_i = \mathbf{0}$ in the following theorem.

Lemma 3: Let the flow be updated according to (12) and suppose that $\Delta\mathbf{F}_i \neq \mathbf{0}$, defined in Eq.(12), then the spectral norm of $\|\mathbf{A}_i\| = \sigma(\mathbf{A}_i^\top\mathbf{A}_i)^{\frac{1}{2}}$ follows:

$$\|\mathbf{A}_i\| = 1 - w. \qquad (25)$$

Proof: Let $\mathbf{L}_i = [\mathbf{T}_i, -\sqrt{\lambda}\mathbf{R}^\top]^\top$ and $\Theta_i = \mathbf{L}_i\mathbf{M}_i\mathbf{L}_i^\top$, we can rewrite $\mathbf{A}_i = \mathbf{I} - \omega\mathbf{L}_i\mathbf{M}_i\mathbf{L}_i^\top = \mathbf{I} - \omega\Theta_i$. Inserting $\mathbf{M}_i = (\mathbf{L}_i^\top\mathbf{L}_i)^{-1}$ in Θ_i^2 results in:

$$\begin{aligned}\Theta_i^2 &= \mathbf{L}_i\mathbf{M}_i\mathbf{L}_i^\top\mathbf{L}_i\mathbf{M}_i\mathbf{L}_i^\top\\ &= \mathbf{L}_i(\mathbf{L}_i^\top\mathbf{L}_i)^{-1}\mathbf{L}_i^\top\mathbf{L}_i\mathbf{M}_i\mathbf{L}_i^\top\\ &= \mathbf{L}_i\mathbf{M}_i\mathbf{L}_i^\top = \Theta_i.\end{aligned}$$

Let u and κ_Θ be the eigenvector and the eigenvalue of Θ_i, then $\Theta_i u = \Theta_i^2 u$ implies that $\kappa_\Theta u = \kappa_\Theta^2 u$. Hence $\kappa_\Theta \in \{0, 1\}$ and the eigenvalues of $\mathbf{A}_i$ are $\kappa_\mathbf{A} \in \{1, 1-\omega\}$. Furthermore, given that $\mathbf{M}_i$ is symmetric, then Θ_i is also symmetric. Hence $\mathbf{A}_i$ is symmetric. Given that the eigenvalues of $\mathbf{A}_i$ are $\kappa_\mathbf{A} \in \{1, 1-\omega\} > 0$ and $\mathbf{A}_i$ is symmetric, then $\mathbf{A}_i$ is positive definite. Further, $\mathbf{M}_i$ has full rank which implies that $\kappa_\mathbf{A} = 1$ only if $\Delta\mathbf{F}_i = \mathbf{L}_i^\top\mathbf{X}_i = \mathbf{0}$. Since we assumed that $\Delta\mathbf{F}_i = \mathbf{L}_i^\top\mathbf{X}_i \neq \mathbf{0}$, we consider the case when $\kappa_\mathbf{A} = 1 - \omega$. Hence $\|\mathbf{A}_i\| = 1 - \omega$. ■

Now we prove the convergence of the RMT algorithm.

Theorem 1: Suppose that Assumption 1 is true then $\|\mathbf{X}_i\| \longrightarrow 0$ when $i \longrightarrow \infty$.

Proof: We show that $\mathbf{X}_i \longrightarrow 0$ when $i \longrightarrow \infty$ when $\Delta\mathbf{F}_i = 0$ and $\Delta\mathbf{F}_i \neq 0$. Insert Eq.(13) in $\mathbf{C}_{i+1}$ leads to:

$$\mathbf{C}_{i+1} = (\mathbf{T}_i - \mathbf{T}_{i+1})^\top((1-\omega)^{i+1}\mathbf{F}_0 + (1-(1-\omega)^{i+1})\mathbf{Y})$$

Consider $\mathbf{T}_i\mathbf{Y}$ and apply $\mathbf{Y} = [\mathbf{Y}_x, \mathbf{Y}_y]$ where $\mathbf{Y}_x = \frac{\hat{r}_x}{t^{\text{tot}}}\mathbf{I}$, $\mathbf{Y}_y = \frac{\hat{r}_y}{t^{\text{tot}}}\mathbf{I}$ and $\hat{r} = [\hat{r}_x, \hat{r}_y]$, then $\mathbf{T}_i\mathbf{Y}$ follows $\mathbf{T}_i^\top\mathbf{Y} = \mathbf{T}_i^\top\mathbf{I}\hat{r} = \sum_k \frac{t_i^k}{t^{\text{tot}}}\hat{r}$. Since $\sum_k t_i^k = \sum_k t_{i+1}^k = t^{\text{tot}}$, then $\mathbf{T}_{i+1}\mathbf{Y} = \mathbf{T}_i\mathbf{Y}$ and $\mathbf{C}_{i+1}$ is simplified to:

$$\mathbf{C}_{i+1} = (1-\omega)^{i+1}(\mathbf{T}_i - \mathbf{T}_{i+1})^\top\mathbf{F}_0 \qquad (26)$$

We rewrite Eq.(19) using $\mathbf{B}_i = [\mathbf{C}_{i+1}, \mathbf{0}]^\top$ and $\mathbf{X}_0$:

$$\mathbf{X}_{i+1} = \mathbf{A}_i\mathbf{X}_i + \mathbf{C}_{i+1} = \prod_{j=0}^{i}\mathbf{A}_j\mathbf{X}_0 + \sum_{j=1}^{i+1}\prod_{l=j}^{i}\mathbf{A}_l\mathbf{C}_j \qquad (27)$$

Insert Eq.(26) in (27) results in the following dynamics:

$$\mathbf{X}_{i+1} = \prod_{j=0}^{i} \mathbf{A}_j \mathbf{X}_0 + \sum_{j=1}^{i+1} \prod_{l=j}^{i} \mathbf{A}_l \mathbf{C}_j \tag{28}$$
$$= \prod_{j=0}^{i} \mathbf{A}_j \mathbf{X}_0 + \sum_{j=1}^{i+1} \beta_j \prod_{l=j}^{i} \mathbf{A}_l (\mathbf{T}_{j-1} - \mathbf{T}_j)^\top \mathbf{F}_0$$

where $\beta_j = (1-\omega)^j$. Consider $\|\mathbf{T}_i - \mathbf{T}_{i+1}\|$ and notice that $\|T_j\|^2 = \sum_{k=1}^{f} (t_j^k)^2 \leq (\sum_{k=1}^{f} t_j^k)^2 = (t^{\text{tot}})^2$. Thus an upper bound $\|\mathbf{T}_i - \mathbf{T}_{i+1}\|$ follows:

$$\|\mathbf{T}_i - \mathbf{T}_{i+1}\| \leq \|\mathbf{T}_i\| + \|\mathbf{T}_{i+1}\| \leq t^{\text{tot}} + t^{\text{tot}}$$

We denote with $\sigma = 2t^{\text{tot}}$ an upper bound for $\|\mathbf{T}_i - \mathbf{T}_{i+1}\|$ and we apply Lemma 3, which implies that $\|\mathbf{A}_j\| = 1 - w$ when $\Delta\mathbf{F}_j \neq \mathbf{0}$. Finally an upper bound for $\|\mathbf{X}_{i+1}\|$ follows:

$$\|\mathbf{X}_{i+1}\| \leq (1-w)^{i+1}\|\mathbf{X}_0\| + \sigma \sum_{j=1}^{i+1} (1-\omega)^j (1-w)^{i-j+1} \|\mathbf{F}_0\|$$
$$\leq (1-w)^{i+1}\|\mathbf{X}_0\| + \sigma(i+1)(1-\omega)^{i+1}\|\mathbf{F}_0\|$$

Since $(1-\omega)^{i+1} \longrightarrow 0$, then $(1-w)^{i+1}\|\mathbf{X}_0\| \longrightarrow 0$ when $i \longrightarrow \infty$. Considering the second term in (29), we use the Maclaurin series theorem, to show that: $\sum_{i=1}^{\infty} i\beta^i = \frac{\beta}{(1-\beta)^2}$ with $\beta = 1-\omega$. Hence the series $\sum_{i=1}^{\infty} i\beta^i$ converges. Further Theorem 1 from chapter 11 in [17] states that if $\sum_{i=1}^{\infty} i\beta^i$ converges, then $\lim_{i \longrightarrow \infty} i\beta^i = 0$.

Hence, $(i+1)(1-\omega)^{i+1} \longrightarrow 0$ when $i \longrightarrow \infty$. As σ is bounded, then $\sigma(i+1)(1-\omega)^{i+1} \longrightarrow 0$ when $i \longrightarrow \infty$, and accordingly $\|\mathbf{X}_i\| \longrightarrow 0$ when $i \longrightarrow \infty$ if $\Delta\mathbf{F}_i = (\mathbf{T}_i\mathbf{d}_i - \lambda\mathbf{R}^\top\mathbf{R}\mathbf{F}_i) \neq \mathbf{0}$.

We consider in the following the case $\Delta\mathbf{F}_i = \mathbf{0}$. Hence, $(\mathbf{T}_i\mathbf{d}_i = \lambda\mathbf{R}^\top\mathbf{R}\mathbf{F}_i)$. Apply $\mathbf{R}^\top\mathbf{R}\mathbf{I} = \mathbf{0}$ and $\mathbf{T}_i^\top\mathbf{I} = t^{\text{tot}}$:

$$\mathbf{I}^\top\mathbf{T}_i\mathbf{d}_i = t^{\text{tot}}\mathbf{d}_i = \lambda\mathbf{I}^\top\mathbf{R}^\top\mathbf{R}\mathbf{F}_i = \mathbf{0} \tag{29}$$

Hence $\mathbf{d}_i = \mathbf{0}$ and $\mathbf{R}\mathbf{F}_i = \mathbf{0}$ hold.

Recall that $\mathbf{X}_i = [\mathbf{d}_i, \sqrt{\lambda}\mathbf{R}\mathbf{F}_i]^\top$, then we conclude from the two cases that $\|\mathbf{X}_i\| \longrightarrow 0$ when $i \longrightarrow \infty$. ■

V. Simulation Results

In this section, we validate the RMT algorithm in (12) for the multiple vehicle scenario and compare it with the parametric MT algorithm introduced in [7]. Notice that we proved in the theoretical analysis that the predicted flow converges to a constant flow and the MT error $d_i \longrightarrow 0$ in the single vehicle case. The simulation for multi vehicles shows that the RMT algorithm converges to a different equilibrium, where the predicted flow is non-uniform field and $\mathbf{d} \neq 0$.

Consider a square region D discretized in 100 cells by a uniform cartesian grid. We simulate a time-invariant cyclonic flow field modeled by:

$$F_x = \frac{-ay}{2\pi\sqrt{x^2+y^2}}, \quad F_y = \frac{ax}{2\pi\sqrt{x^2+y^2}}$$

Consider the parametric MT, we use 100 Gaussian radial basis functions (GRBF) to model the flow field. Let $\phi_j(r^k)$ be the GRBF with c_j is the center, σ_j is the width of the j.th GRBF and $\eta_j \in \mathbf{R}^2$ the corresponding parameter. We denote with r^k is the center of the k.th cell, then the flow vector F^k in the grid cell C^k is modeled as $F^k = \sum_{j=1}^{100} \eta_j \exp(\frac{-\|\mathrm{r}-\mathrm{c_j}\|^2}{2\sigma_j^2})$. Given c_j and σ_j, designed in [7], we use the parametric MT algorithm to estimate η_j.

We navigate 18 vehicles in the domain D for observation time horizon $t^{\text{tot}} = 1$ hour, where the first 9 AUVs travel from the left of the domain to the right and the other 9 from the bottom to the top. We define the control speed $\|S\| = 0.5m/s$,the time step $\Delta t = 1s$ and we use a first order particle model to simulate the AUV motion $r^{j,k} = r^{j,k-1} + (S^j + F(r^{j,k-1}))\Delta t$. After we collect the simulated final positions, we run the parametric MT algorithm, derived in [7] and the RMT algorithm. The estimated flow is initially null for both algorithms. The AUV trajectory is traced at iteration i using the current estimate of the flow field $\mathbf{F}_i$. Further, the MT error $\mathbf{d}_i$ and the travel time matrix $\mathbf{T}_i$ are computed in the trajectory tracing step to update the flow estimate in the inverse step. We choose $a = 2.5m/s$, the step size $\omega = 0.1$ and the regularization parameter $\lambda = 0.1$. We run the RMT and the parametric MT algorithms until the MT error is $\|\mathbf{d}_i\| \leq 10^{-2}m$. Let F^k be the discrete value of the true flow in cell C^k, we define the estimation error in C^k as $e^k = \tilde{F}^k - F^k$ and compute the root-mean square RMS $\delta_F = \sqrt{\frac{\sum_{k=1}^{100} \|\tilde{F}^k - F^k\|^2}{100}}$ to compare the RMT and parametric MT algorithm.

Figure 2 shows that parametric MT flow error δ_F has higher RMS than the RMT flow error, which aligns with Figure 3. The RMT algorithm outperforms the parametric MT in the center of the domain D, where the flow field is highly varying. The GRBF parametrization favors more a uniform flow field in comparison with the Laplacian regularization. Therefore, the RMT algorithm captures the spatial flow variation better than the parametric MT, in particular in the right half of the field, see Fig.2. While the RMT flow estimate has similar direction as the true flow field, the parametric predicted flow field is in the opposite direction of the true flow field. Further, Fig.3 shows that parametric MT has a lower convergence rate in comparison with the RMT and the overshoot of the RMS error of parametric MT is higher than the overshoot of RMT. Finally, we deduce from Fig.3 that the RMS error of RMT, $0.155m/s$ is less than half of the RMS error of parametric MT $0.367m/s$. The regularization term $\lambda\mathbf{R}^\top\mathbf{R}$ in the RMT algorithm allows us to compute the exact inverse of the travel time matrix, $(\mathbf{T}_i{}^\top\mathbf{T}_i + \lambda\mathbf{R}^\top\mathbf{R})^{-1}$. For the parametric Mt algorithm, the travel time matrix is singular and we are forced to approximate the inverse, $\frac{1}{\|\mathbf{T}_i\|^2}$, see [7] for more details. Further, increasing the step size for parametric MT leads to divergence of the MT error. Therefore, the RMT convergence rate is higher than the parametric MT convergence rate.

In order to study the effect of regularization weight on the estimation, we run the RMT algorithm with different values of λ and we compare it to the MT algorithm, presented in Eq.(8). Fig.4 shows that the RMT algorithm outperforms the MT algorithm. The MT RMS is more than double the RMS

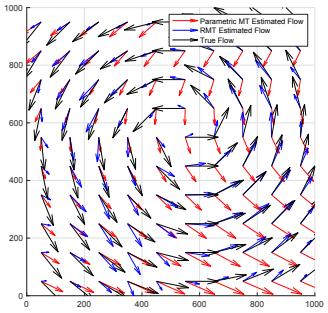

Fig. 2: A simulated true flow (black) $\|F\| = 0.3975$, RMT predicted flow field (blue) and MT predicted flow field (red).

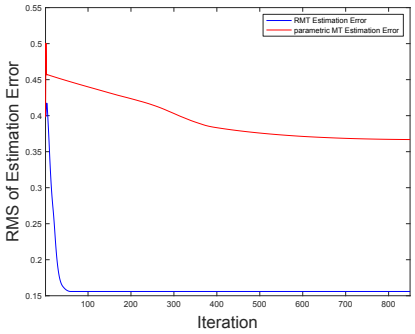

Fig. 3: RMS Error of flow estimation with $\omega = 0.1, \lambda = 0.1$.

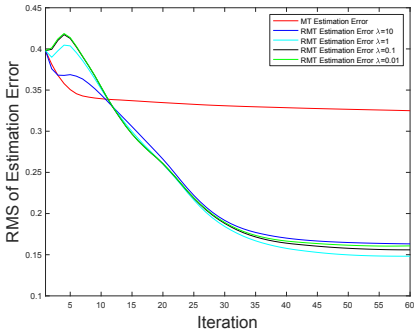

Fig. 4: RMS Error of flow estimation for different λ with $\omega = 0.1$ and $\|F\| = 0.397 m/s$.

of RMT algorithm. Further, we notice that increasing λ leads to less overshoot, which is expected as the higher λ is, the smoother is the flow field. However, since the cyclonic flow field is highly varying, we notice that the RMS error is worst when $\lambda = 10$. This can be explained by the fact that the discrete true flow field is non smooth. However, when we choose $\lambda \leq 1$, increasing λ from 0.01 to 1 leads to better RMS error. Hence, we conclude that the choice of λ is a trade-off between overfitting, as RMT algorithm outperforms MT algorithm, and underfitting as increasing λ above some threshold can degrade the accuracy of the estimation.

VI. CONCLUSIONS

In this paper, we extended the MT algorithm with the Laplacian regularization to alleviate the ill-posedness of the inverse step. We derived the RMT algorithm for multiple AUVs and we studied the dynamics of the RMT error. This allowed to prove the convergence of the RMT algorithm in the single vehicle case. The simulation of the algorithm for multiple vehicles showed that the Laplacian regularization increases the convergence rate and improves the estimation in comaprison with the GRBF parametric MT. In our future work, we would like to explore different regularization techniques, investigate collaborative exploration strategies and incorporate new measurements in the RMT algorithm.

REFERENCES

[1] Z. Song and K. Mohseni, "Towards background flow based auv localization," in *Decision and Control (CDC), 2014 IEEE 53rd Annual Conference on*. IEEE, 2014, pp. 6945–6950.

[2] P. Mokhasi, D. Rempfer, and S. Kandala, "Predictive flow-field estimation," *Physica D: Nonlinear Phenomena*, vol. 238, no. 3, pp. 290–308, 2009.

[3] S. A. Randeni P, A. L. Forrest, R. Cossu, Z. Q. Leong, and D. Ranmuthugala, "Determining the horizontal and vertical water velocity components of a turbulent water column using the motion response of an autonomous underwater vehicle," *Journal of Marine Science and Engineering*, vol. 5, no. 3, p. 25, 2017.

[4] L. Merckelbach, R. Briggs, D. Smeed, and G. Griffiths, "Current measurements from autonomous underwater gliders," in *Current Measurement Technology, 2008. CMTC 2008. IEEE/OES 9th Working Conference on*. IEEE, 2008, pp. 61–67.

[5] K. M. B. Lee, C. Yoo, B. Hollings, S. Anstee, S. Huang, and R. Fitch, "Online estimation of ocean current from sparse gps data for underwater vehicles," in *2019 International Conference on Robotics and Automation (ICRA)*. IEEE, 2019, pp. 3443–3449.

[6] H. Bai, "Motion-dependent estimation of a spatial vector field with multiple vehicles," in *2018 IEEE Conference on Decision and Control (CDC)*. IEEE, 2018, pp. 1379–1384.

[7] D. Chang, W. Wu, C. R. Edwards, and F. Zhang, "Motion tomography: Mapping flow fields using autonomous underwater vehicles," *International Journal of Robotics Research*, vol. 36, no. 3, pp. 320–336, 2017.

[8] M. Ouerghi and F. Zhang, "An improved algorithm for motion tomography by incorporating vehicle travel time," in *2018 Annual American Control Conference (ACC)*. IEEE, 2018, pp. 1907–1912.

[9] A. Kirsch and A. Rieder, "Seismic tomography is locally ill-posed," *Inverse Problems*, vol. 30, no. 12, p. 125001, 2014.

[10] M. Richter, *Inverse problems: Basics, theory and applications in geophysics*. Birkhäuser, 2016.

[11] M. Benning and M. Burger, "Modern regularization methods for inverse problems," *Acta Numerica*, vol. 27, pp. 1–111, 2018.

[12] P. Mojabi and J. LoVetri, "Overview and classification of some regularization techniques for the gauss-newton inversion method applied to inverse scattering problems," *IEEE Transactions on Antennas and Propagation*, vol. 57, no. 9, pp. 2658–2665, 2009.

[13] M. Ouerghi, S. Maxon, and F. Zhang, "The convergence of trajectory tracing for motion tomography algorithm," *IEEE T-RO 20-0218, under review*, 2020.

[14] M. Belkin, P. Niyogi, and V. Sindhwani, "Manifold regularization: A geometric framework for learning from labeled and unlabeled examples," *Journal of machine learning research*, vol. 7, no. Nov, pp. 2399–2434, 2006.

[15] X. J. Zhu, "Semi-supervised learning literature survey," University of Wisconsin-Madison Department of Computer Sciences, Tech. Rep., 2005.

[16] J. R. Kuttler and V. G. Sigillito, "Eigenvalues of the laplacian in two dimensions," *Siam Review*, vol. 26, no. 2, pp. 163–193, 1984.

[17] D. Guichard, H. J. Keisler, and N. Koblitz, *Calculus-Early Transcendentals*. BCcampus Open Textbooks, 2013.